Deposition and Characterization of Core-Shell $SrTiO_3$ Material for Dye Sensitized Photoelectrosynthesis Cell Applications

By

Caroline Reilly

Senior Honors Thesis

Chemistry

University of North Carolina at Chapel Hill

April 19, 2017

Approved:

_____

Thomas J. Meyer, Thesis Advisor

Jillian L. Dempsey, Reader

Alexander J. M. Miller, Reader

Abstract

A core shell semiconductor strategy for solar water splitting is exploited here based on a Dye Sensitized Photoelectrosynthesis Cell approach. Strontium titanate ($SrTiO_3$) shows promise as a new material due to the wide band gap and water-splitting capacity under light, without any applied bias. Films on fluorine-doped tin oxide substrate, were chemically deposited using $SrTiO_3$ solution as a shell on high surface area indium tin oxide as the core material. After annealing, this new core-shell material was characterized through Mott-Schottky, scanning electron microscopy, transmission electron microscopy, and energy dispersive spectroscopy. Dye loading on the substrates in the presence of thiolate/disulfide showed photocurrent responses up to 300 $\mu A/cm^2$. The core-shell $SrTiO_3$ films were then loaded with dye and constructed into dye sensitized solar cells. Devices were tested through incident photon to current efficiency, linear sweep voltammetry, and electrochemical impedance spectroscopy under 1 sun illumination and with 0 V applied bias. Efficiencies on the order of 0.002% were recorded.

Introduction

Dye-sensitized solar cells (DSSCs) have been a prominent topic in solar energy research for decades, as an alternative to conventional silicon solar cells. DSSCs utilize a transparent conducting oxide (TCO) and a wide bandgap semiconductor on which a dye is loaded.[1] The dye is excited by light and, for the photoanode, injects an electron into the conduction band of the semiconductor, which then transports the electron to the TCO to do work (Figure 1). Although DSSCs have not reached the commercial efficiency shown by silicon solar cells, the potential applications of thin film, semitransparent DSSCs are more widespread.[2]

Further, the connection between DSSCs and dye-sensitized photoelectrochemical cells (DSPECs) have continued to make research into new materials for DSSCs worthwhile. DSPECs form fuels such as hydrogen and methane by using sunlight to split water and reduce carbon dioxide, respectively.[3] The photoanode side of DSPECs is where water splitting takes place, producing hydrogen, which has been promoted solar fuel for the

upcoming renewable energy surge.[4] New materials and configurations proven effective in DSSCs can be considered as candidates for these DSPEC devices. This study looks to further the goal of the UNC Energy Frontier Research Center: Center for Solar Fuels. That goal is to make tandem DSPECs that combine the photoanode side with the photocathode side to drive both oxidation and reduction simultaneously with two electrode tandem devices.[5]

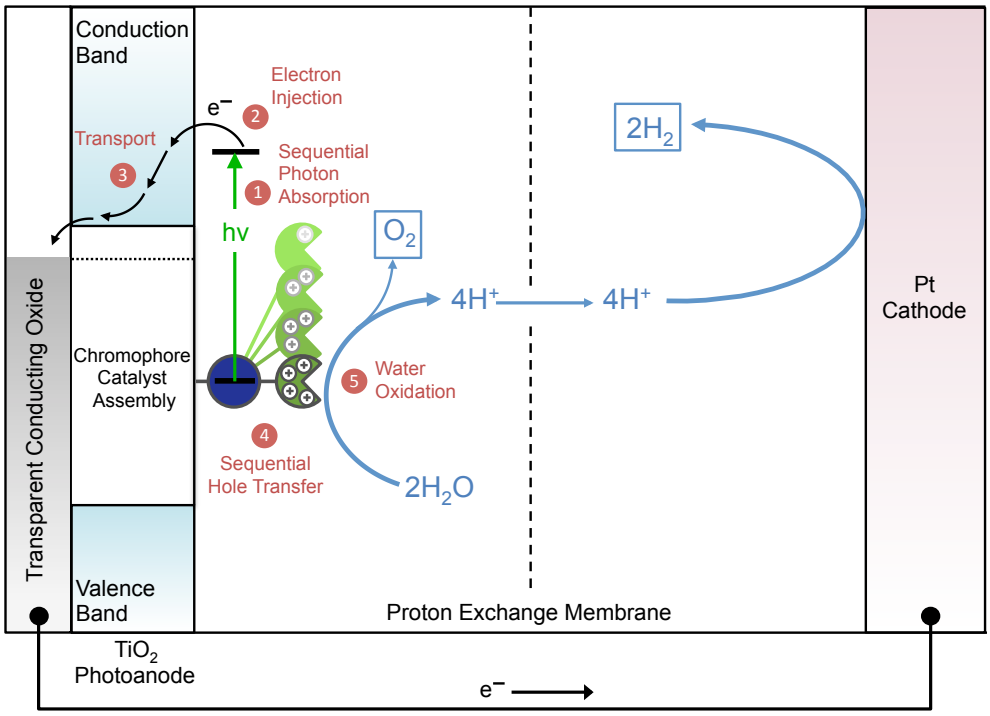

Figure 1. DSPEC two-electrode schematic showing water oxidation by a catalyst at the photoanode and hydrogen evolution at the Pt counter electrode.[3]

Many studies have focused on TiO_2 as the metal oxide for the photoanode side, as a wide bandgap semiconductor for electron injection.[6–8] However, photocurrent response from TiO_2 can only be achieved with an applied bias versus the platinum cathode. Strontium titanate ($SrTiO_3$, STO) has been suggested as an alternative metal oxide to TiO_2, with the ability to operate at zero bias conditions.[9] A recent study from the Lopez group showed that flat STO films grown by pulsed laser deposition (PLD) could make DSSCs

producing a photocurrent with no applied bias.[10] However, the photocurrent achieved in those studies under the best conditions was only 350 nA/cm^2.

Improvements have been made to TiO_2 devices, with devices of high surface area TiO_2 using core-shell structures proving more efficient.[6] In the core-shell approach, the wide bandgap semiconductor is applied on a film of nanoparticles of another semiconductor such that the shell material coats the nanoparticles. The conduction band edge of the core material is below that of the shell material, allowing for electron transport from the shell to the core but an energetic barrier in the opposing direction, minimizing back electron transfer. Back electron transfer by electrons from the semiconductor returning to reduce the dye is a large reason for loss of efficiency in DSSC systems. By varying the shell thickness, it is possible to find an optimal thickness to minimize back electron transfer. Mechanisms for back electron transfer favor recombination within the shell in thick shells and tunneling from the core to the dye in thin shells, such that balancing the two factors can lead to more efficient devices.[11] The core-shell approach is applied in this study to STO films, by using small particle size indium-doped tin oxide (nanoITO) coated in a shell of STO. While TiO_2 core-shell devices have used atomic layer deposition (ALD) in order to create conformal films of TiO_2 encasing nanoITO particles, similar methods have proved ineffective in creating STO films. This study will utilize solution-based drop casting methods for deposition STO films in order to create pseudo core-shell nanoITO-STO DSSC devices as a proof of concept for the application of STO to DSPECs.

Various porphyrin dyes were used in this study, as shown in Scheme 1. The phosphonate group on each dye provides an attachment method to the semiconductor surface.[12] Dye 1 was chosen due to being used in flat STO studies, as photocurrents measured with this dye could be directly compared to those from the previous studies.[10] Dye 2 is another porphyrin dye that was chosen for similarity to Dye 3, which has a ruthenium based catalyst covalently attached to the porphyrin ring that could be used for water splitting. Dye 1 was ineffective for use in DSSCs, and therefore devices were constructed only from Dye 2 and Dye 3.

An aqueous electrolyte was used in this study, with the thiolate/disulfide redox couple in Scheme 2.[13] This redox couple serves in place of the iodide/triiodide redox couple typically utilized in non-aqueous electrolytes in DSSCs.[14] The switch to aqueous

electrolytes serves to test DSSCs in an environment closer to that of DSPEC devices, which need to be in the presence of water in order to enable water splitting and hydrogen evolution. This electrolyte will allow for rapid regeneration of the oxidized dye and improvement in photocurrent responses. In conjunction with the use of more suitable dyes and the core-shell approach, STO DSSCs constructed in this study should show higher efficiencies and better performance over previous STO films, while providing photocurrent response at no applied bias conditions.

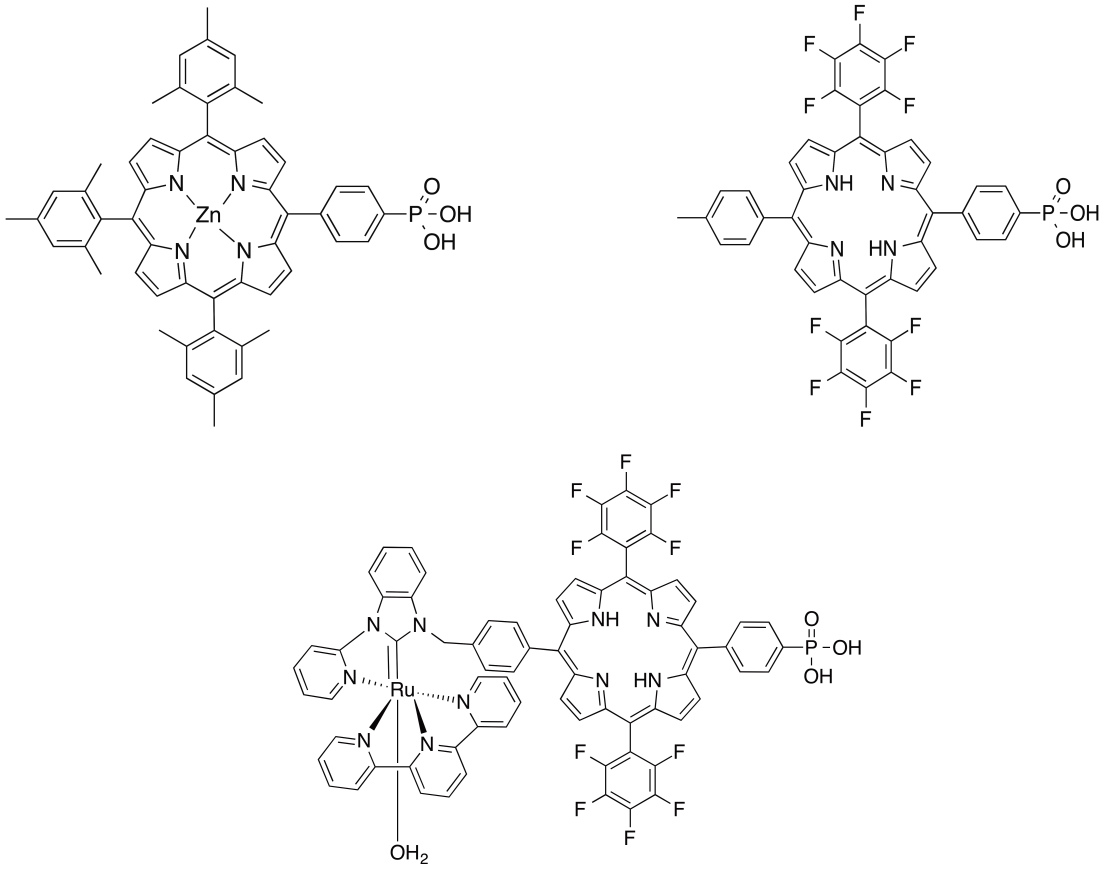

Scheme 1. Three porphyrin dyes studied in this paper; (top left) Dye 1, (top right) Dye 2, (bottom) Dye 3

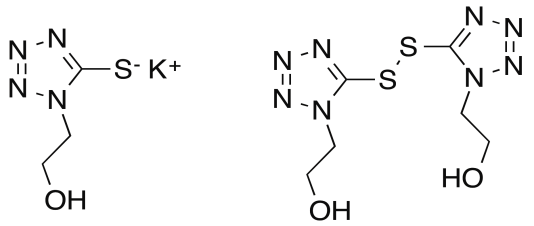

Scheme 2. Thiolate/disulfide electrolyte; 1-(2-hydroxyethyl)-5-mercaptotetrazole potassium salt and 1-(2-hydroxyethyl)-5-mercaptotetrazole dimer

Results

Deposition and characterization of STO films

Chemical deposition by solution based methods was explored in this work. Similar solution depositions have been found successful for other materials such as lead zirconate titanate.[15,16] Figure 2 indicates formation of STO on nanoITO substrates following 50 drops of solution allowed to dry on the film, as indicated by TEM EDS. The insert in Figure 2 shows another nanoITO substrate that was rotated in a vial of solution for several hours, showing no signs of STO deposition.

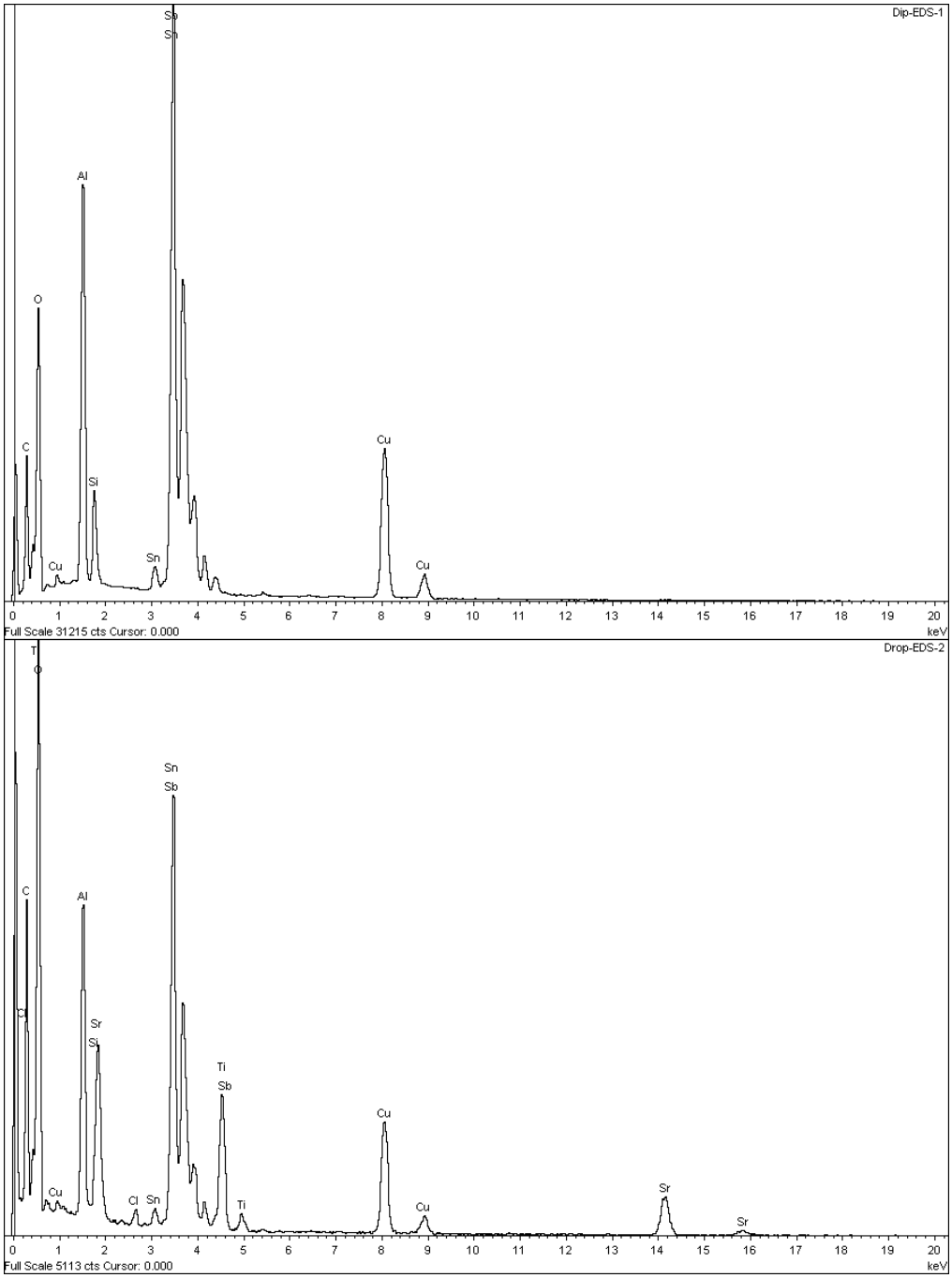

Figure 2. EDS showing sample with 50 drops of STO solution and (insert) sample rolled in solution

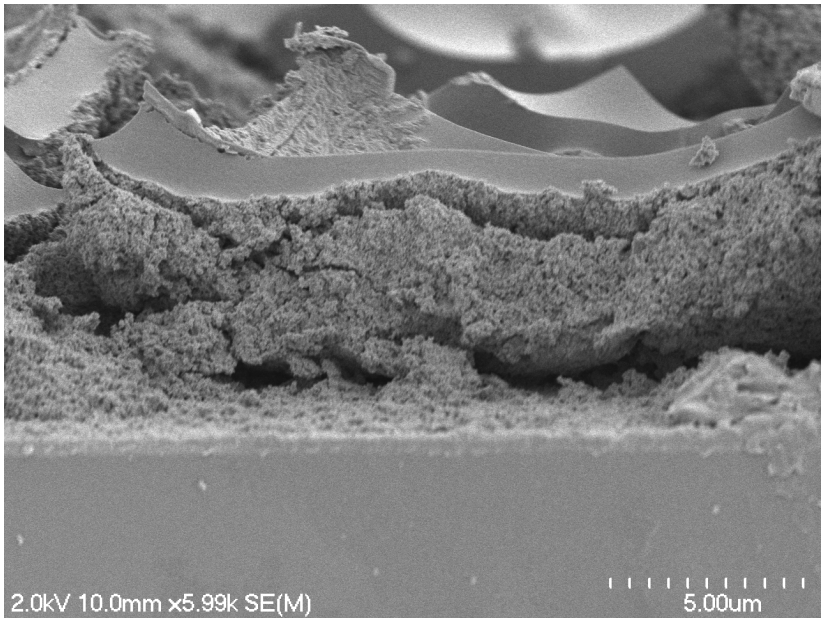

Figure 3. Cross-sectional SEM of nanoITO film with 50 drops of STO solution

Although 50 drops of solution gave clear indication by TEM that STO had formed, the nanoITO film began to peel off of the FTO surface after being disturbed in the drying process (Figure 3). The nanoITO substrates were initially prepared though the use of an ethanol based suspension, therefore the ethanol in the strontium titanate solution caused the peeling up of the nanoITO. By switching to the controlled evaporation system described previously, one large drop could be placed on the nanoITO substrate, and the evaporation process did not disturb the nanoITO film (Figure 4). In order to achieve a covering of the nanoITO material uniformly by the STO, a seeding layer of ALD Al_2O_3 was used in order to provide a beginning shell for the STO to adhere.

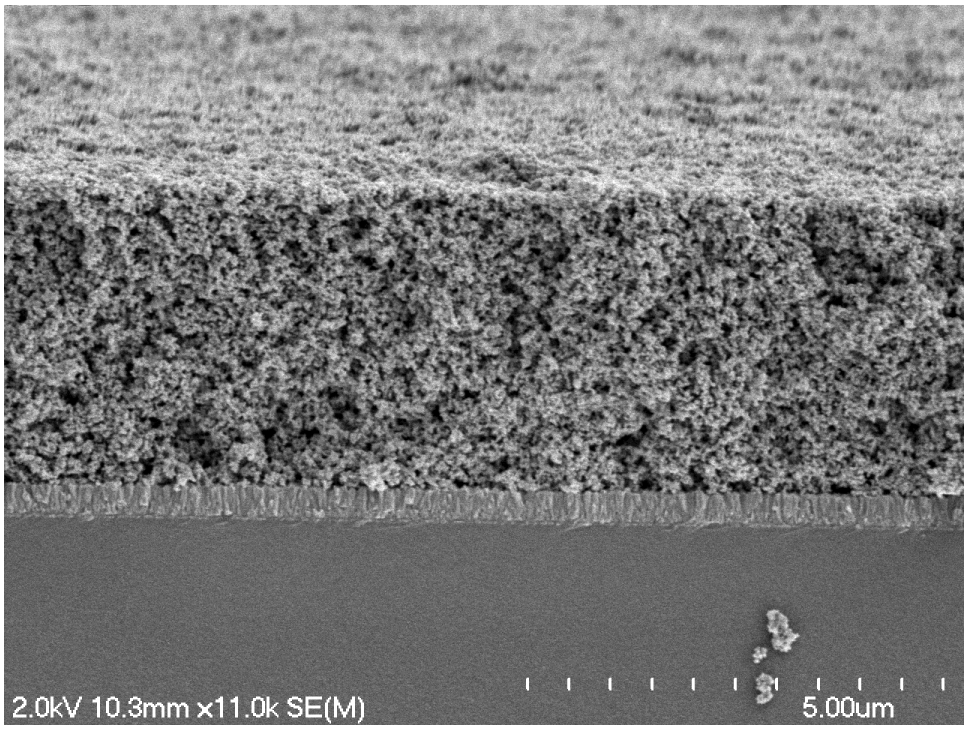

Figure 4. Cross-sectional SEM image of glass (bottom), FTO (lighter film), and nanoITO with Al_2O_3 and STO, showing a 3.5 nm total film thickness.

While ALD produced conformal shell films on the nanoparticle core, previous work has shown that solution based methods such as dip coating produce films with shell structures that do not uniformly cover the core material.[17] This non-uniformity of the film was viewed through TEM imaging of the substrate, as in Figure 5. A conformal shell film was not expected due to the solution based deposition. The STO did cover throughout the nanoITO film, as can be seen by the strontium and titanium presence throughout the material in TEM mapping EDS in Figure 6.

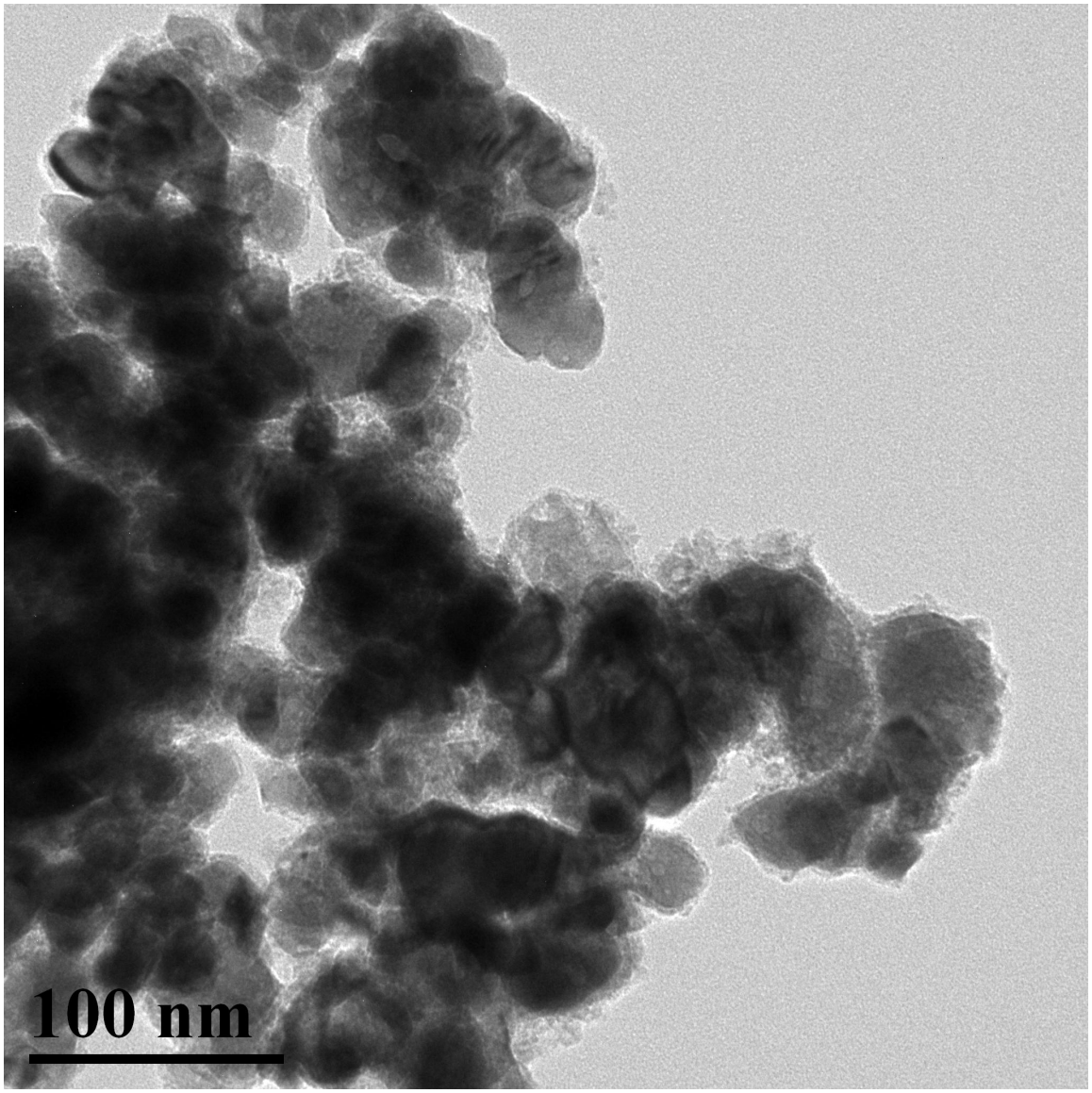

Figure 5. TEM image of film scraped onto copper tape, showing nanoITO particles (~20 nm) with Al_2O_3 and STO smaller shell particles around edges of nanoITO, film treated with two drops of STO solution.

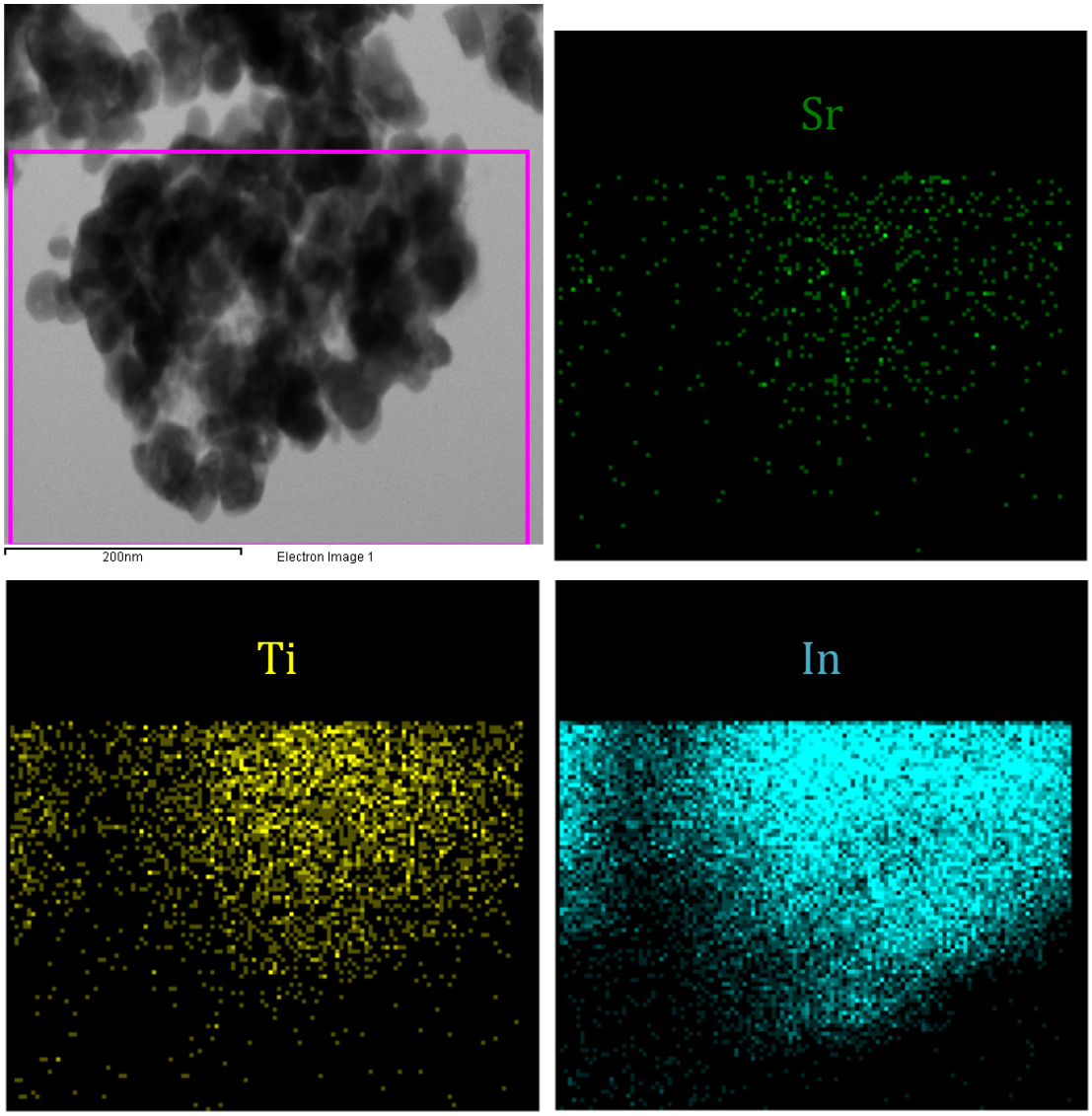

Figure 6. TEM EDS mapping of elements in core-shell structure for one drop STO film scraped from FTO substrate; yellow – Ti, green – Sr, cyan – In

Substrates were created with nanoITO, nanoITO/Al_2O_3, nanoITO/STO, and nanoITO/Al_2O_3/STO, annealed at 300°C, and loaded with RuP dye overnight. At pH 1, these substrates were illuminated and the photocurrent response was measured in Figure 7. It was confirmed that the substrates without STO did not give a photocurrent response, and the substrate with the Al_2O_3 seeding layer performed better than the substrate without the seeding layer.

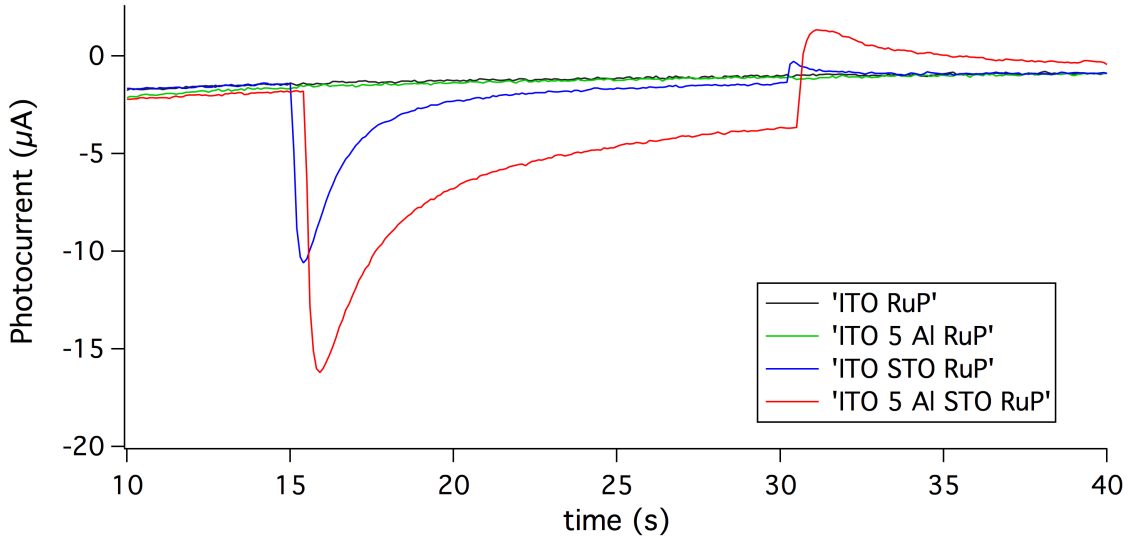

Figure 7. Photocurrent measurements with 445 nm light source in pH 1 with RuP dye on films, ITO/RuP, ITO/Al_2O_3/RuP, ITO/STO/RuP, ITO/Al_2O_3/STO/RuP; three electrode measurements

Substrates of nanoITO on FTO with Al_2O_3 and STO annealed at 500°C under H_2 were loaded with the three dyes to be tested in this study, with the loading over time of the substrates monitored by UV-Vis at 10 minute intervals until all three substrates reached maximum dye loading (Figure 8).

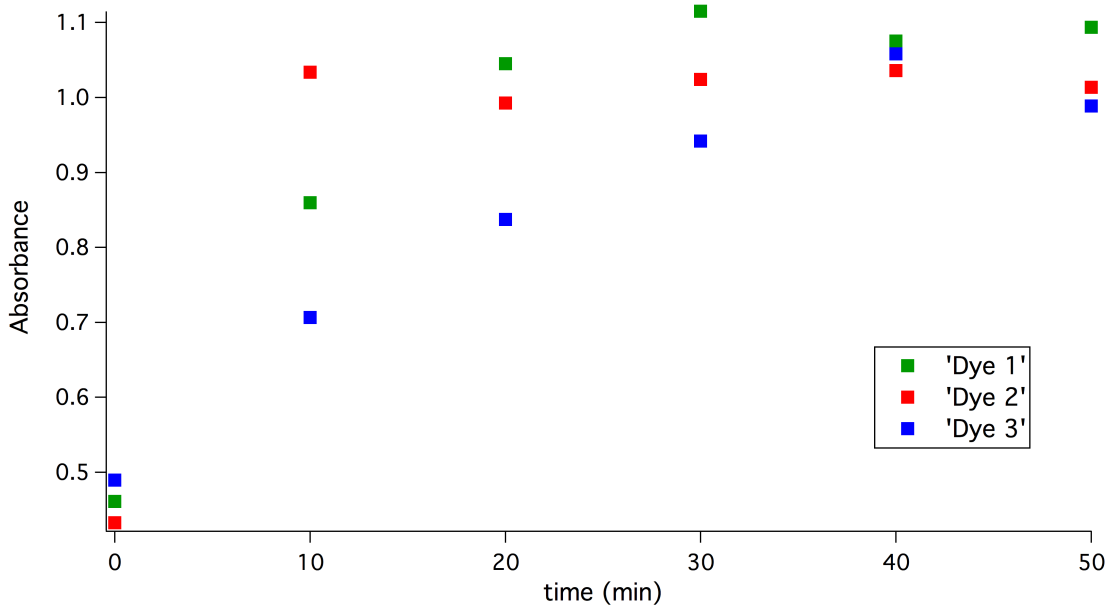

Figure 8. Isotherm showing loading of dyes over time for a set of films, UV-Vis taken every 10 minutes for 50 minutes total, max absorption peak recorded at 556 nm for Dye 1, 513 nm for Dye 2 and Dye 3.

Electrochemical analysis of substrates

The addition of the thiolate/disulfide redox couple to the electrolyte solution greatly increased the dye activity by illumination as seen in the cyclic voltammagrams (Figure 9). Figure 10 showed that the addition of the regenerative couple not only increased the photocurrent, but also caused the photocurrent to be sustained over a longer period of time in the case of Dye 3.

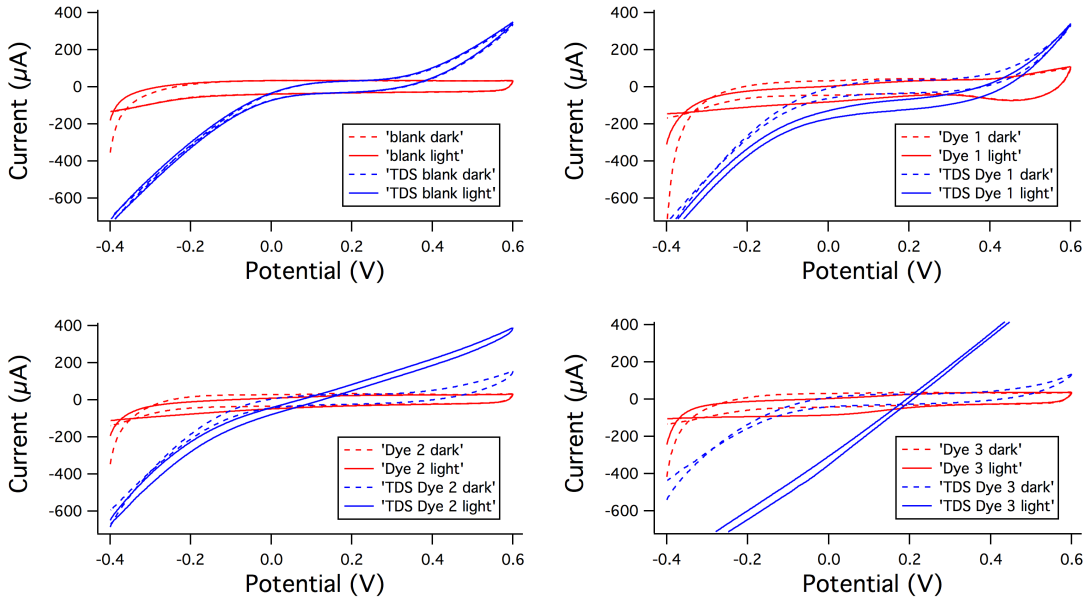

Figure 9. Cyclic voltammetry under illumination (1 sun) and in the dark, -0.4 V to 0.6 V at 10 mV/s, on FTO/nanoITO/Al_2O_3/STO with (top left) no dye, (top right) Dye 1, (bottom left) Dye 2, (bottom right) Dye 3; in pH 5, with and without additives

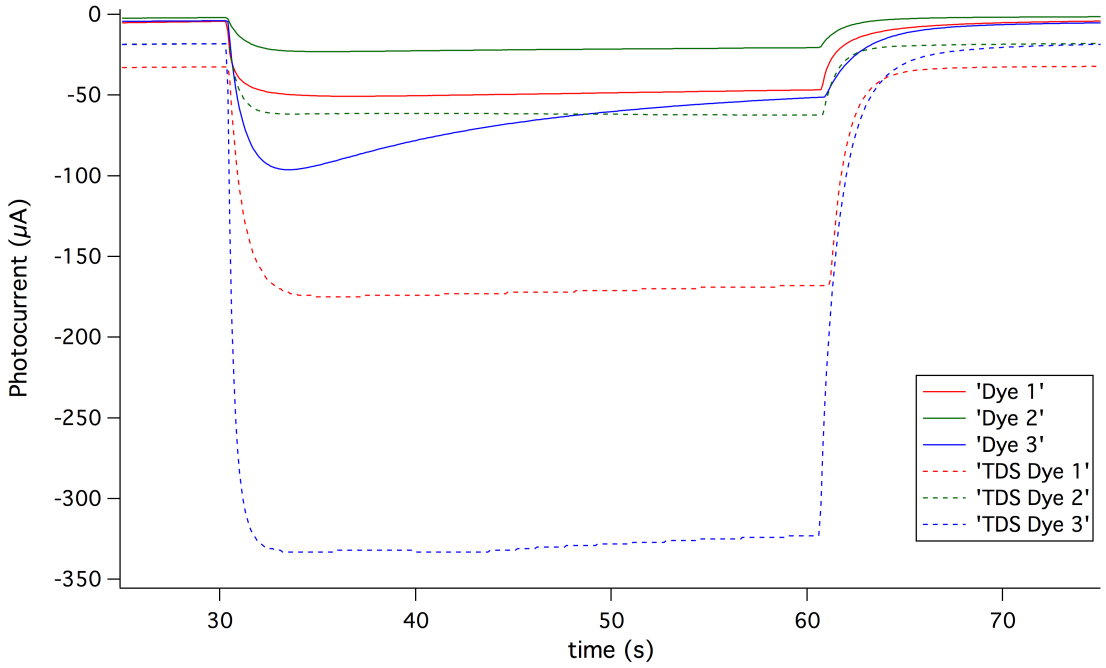

Figure 10. Current versus time curves with illumination under 1 sun for 60 seconds, in pH 5 for all dyes with and without additives

DSSC devices

Sealed DSSCs were constructed with the dye-loaded substrates, with Dye 2 and Dye 3, as the photoanode versus a platinum counter electrode. Electrochemical impedance curves were measured for each device at no applied bias in the dark and under 1 sun illumination (Figure 11). These were plotted as Nyquist plots in order to view each arc caused by the interfaces of the device (Figure 12).

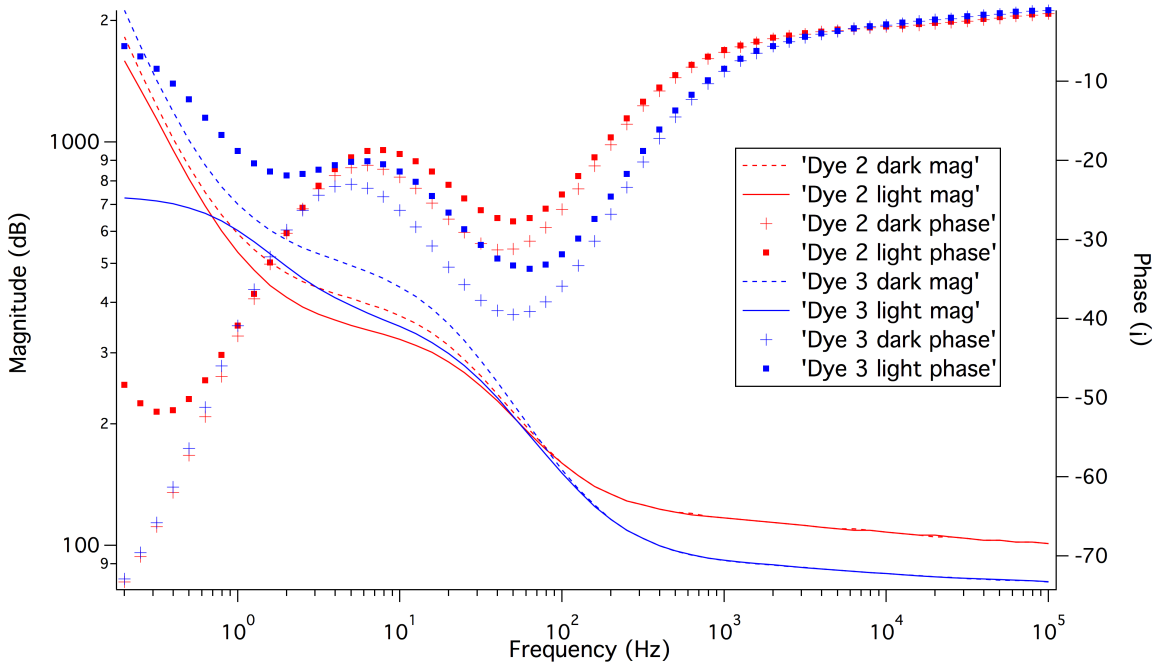

Figure 11. Potentiostatic electrochemical impedance spectroscopy bode plots for DSSCs, in light and dark

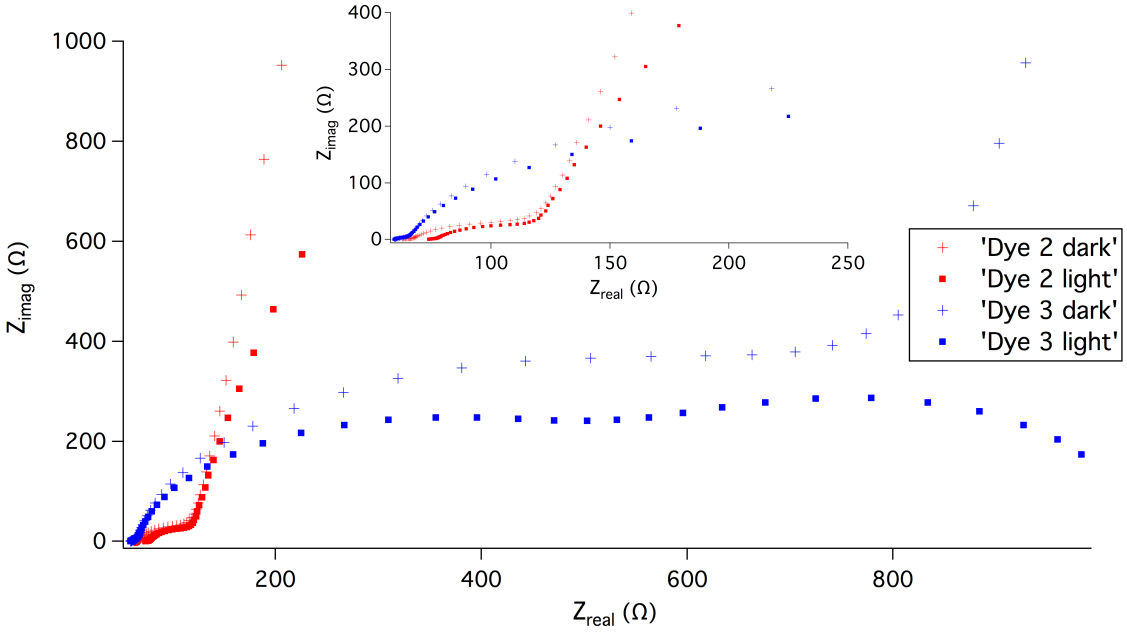

Figure 12. Potentiostatic electrochemical impedance spectroscopy nyquist plots for DSSCs, in light and dark, insert of zoomed in region

Incident photon to current efficiency (IPCE) measurements were made on the DSSCs and compared to the UV-Vis spectra collected for the dyes (Figure 13). Linear sweep voltammagrams (LSV) were also collected in the dark and under 1 sun illumination in order to calculate device efficiencies (Figure 14). The open circuit potential (OCV) between the device electrodes was measured as a function of time when the light was turned off in Figure 15. The V_{OC} measured through LSV was consistent with the potential difference measured between the electrodes by OCV.

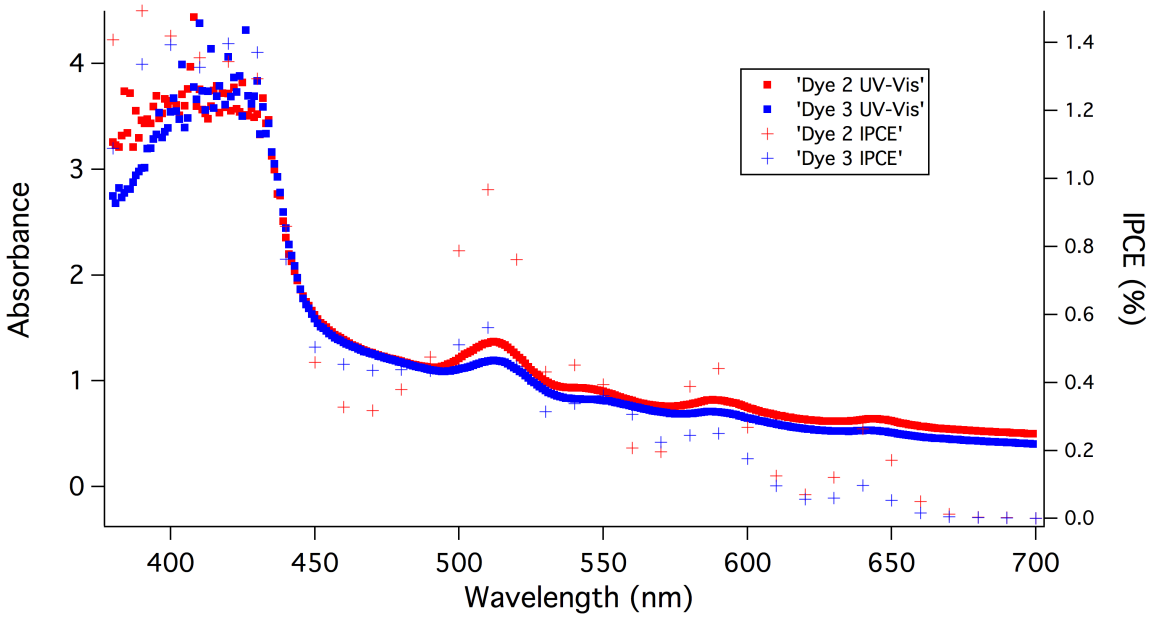

Figure 13. Overlaid UV-Vis and IPCE measurements for DSSCs

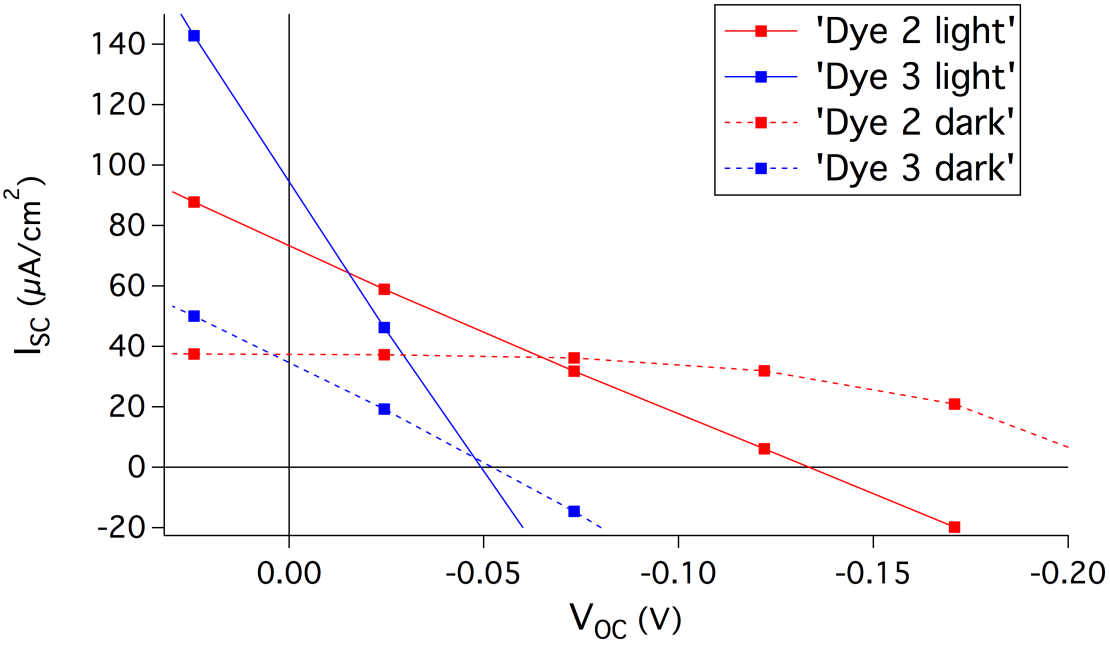

Figure 14. Linear sweep voltammetry for dark and illumination under one sun, DSSCs

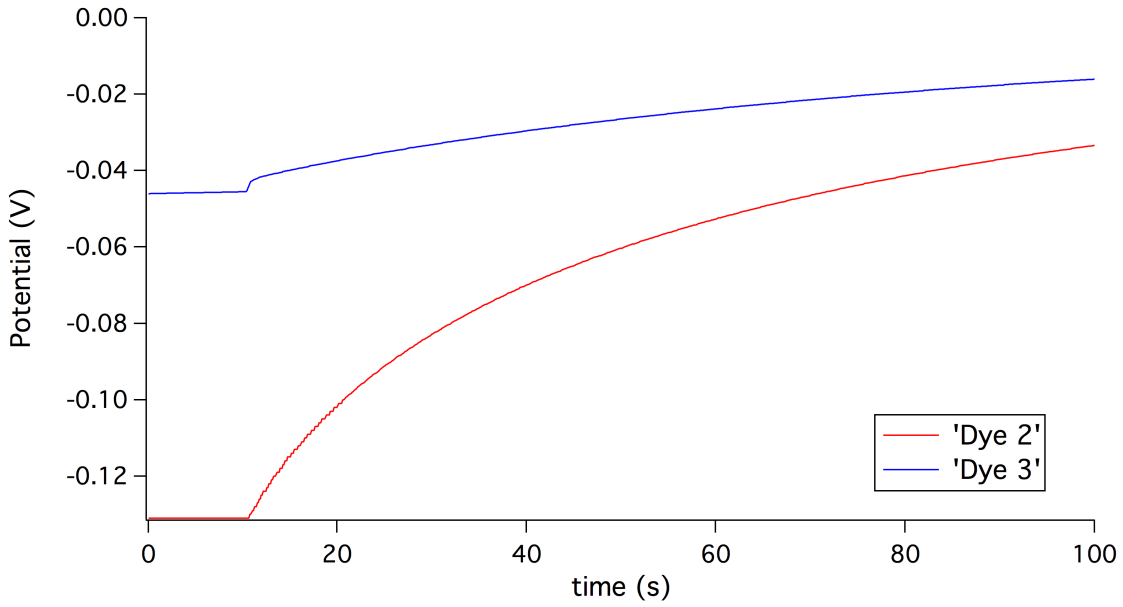

Figure 15. Open circuit voltage decay curves with 1 sun illumination off at 10s for DSSCs

Discussion

Photocurrents

In the flat PLD STO study, photocurrents of 350 nA/cm^2 were achieved with Dye 1 loaded.[10] In this study, photocurrents of 46 μA/cm^2 were found for the same dye, indicating that the new core-shell structure was more effective in producing a photocurrent. With the addition of the thiolate/disulfide couple, photocurrents increased by two to three times. Since the photocurrent measurements in this case were three electrode measurements with a reference electrode, Dye 3 with the attached catalyst compound showed especially high photocurrents due to the catalytic activity. The sustained photocurrent with the addition of the thiolate/disulfide in the case of Dye 3 was attributed to the redox couple being able to regenerate the catalyst after the reaction.

Table 2. Photocurrents in pH 5, μA/cm^2		
Dye	no $T^-/^+DS$	with $T^-/^+DS$
1	- 46	- 142
2	- 21	- 43
3	- 89	- 315

Impedance measurements

The basis for the impedance measurements was the effective chemical impedances and capacitances present at the interfaces in the DSSCs.[18] Upon illumination with light, the excited dye is able to inject electrons into the semiconductor material, effectively lowering the resistance at the interface between the dye and the rest of the substrate. This can be seen through the difference between the impedance data in the dark and under illumination. While complicated models exist to fit the data, this study focused on using a simple method that incorporated three interfaces as parallel RC components and an additional connection resistance between the working electrode photoanode and the platinum counter electrode, as shown in Scheme 3. Gamry Analyst software was used to model and fit the EIS data. The Nyquist plots were used for fitting.

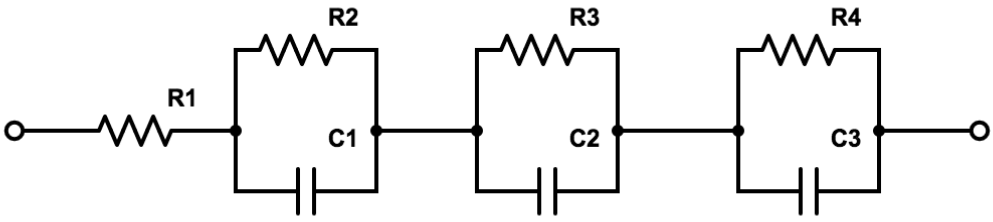

Scheme 3. Electrical model used for Gamry software fitting indicating the effective electronic communication between the electrodes in the DSSCs

The overall impedance of this theoretical model could be determined through the use of Equation 1. The order of the interfaces is electrically unimportant, as the series interfaces simply sum to a total impedance. Lower impedances were ideal for DSSCs under illumination, as voltage equals impedance times current, therefore a lower impedance would produce a higher current for the same potential difference. The data was fit by first using the Gamry AutoFit function based on the input model, then manually adjusting parameters to better fit the arcs of the Nyquist plots. The connectivity resistance determined the starting point along the Z_{real} axis, and each arc in the plot corresponded to one the interfaces. From the data fits in Table 3, it can be seen that the connectivity resistance as well as two of the parallel RC impedances had little change between devices and level of illumination. However, the resistance of the interface between the dye and the STO changed considerably upon illumination. In the case of Dye 2, the resistance became 18% of the initial resistance in the dark and for Dye 3, the resistance in light was 1.3% of the resistance in the dark. These results suggest that Dye 3 is more effective at injection into the semiconductor and allowing more current to flow through the system.

$$Z_{Total}(\omega) = R_1 + \frac{R_2}{j\omega R_2 C_2} + \frac{R_3}{j\omega R_3 C_3} + \frac{R_4}{j\omega R_4 C_4}$$

Equation 1. Impedance calculations for system based on fit model

Table 3. Fitting data from EIS Nyquist plot of DSSCs

Device	R_1	R_2	C_1	R_3	C_2	R_4	C_3
Dye 2 dark	101	15000	350	290	20	15	5
Dye 2 light	101	2700	400	230	20	15	5
Dye 3 dark	81	30000	80	420	7	15	5
Dye 3 light	81	385	200	260	12	10	2

Electron lifetimes and DSSC figures of merit

The lifetime of electrons in the DSSCs was found at each potential on the corresponding open circuit potential decay curves. These decay curves show the regeneration of the excited dye with the electrolyte, providing information about decay processes at the dye-electrolyte interface while effectively ignoring back electron transfer at the semiconductor-dye interface.[19] By using equation 2, the lifetimes were calculated at each point on the curve and plotted in Figure 16. The curve for Dye 2 showed a number of shorter-lived electrons at higher open circuit potentials, and longer lived electrons as the voltage decay continued. Dye 3 indicated a sharp decay followed by a longer lived feature, showing that the initial electron lifetimes were shorter and that there were two decay pathways in the device. Since Dye 3 contained the catalyst, the short lived electrons were from fast regeneration of the catalyst by the electrolyte. Dye 2 having many shorter lived electrons in comparison to Dye 3 also could be justified by the presence of the catalyst in Dye 3 inhibiting electron transfer between the electrolyte and the porphyrin. In Dye 2, the lack of catalyst allowed for better connectivity between the porphyrin and the electrolyte.

$$\tau_n = -\frac{k_B T}{e}\left(\frac{\mathrm{d}V_{OC}}{\mathrm{d}t}\right)^{-1}$$

Equation 2. Finding electron lifetimes as a function of the time derivative of the V_{OC} decay curve.[19]

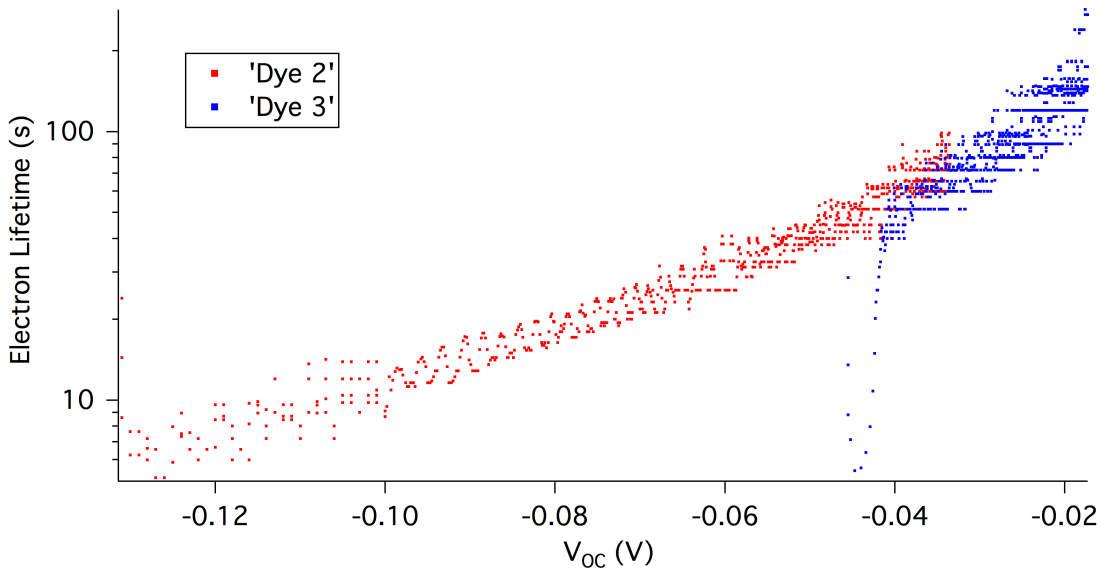

Figure 16. Lifetime of electrons plotted against potential

Short circuit currents, open circuit voltages, and fill factors were obtained from the LSV curves for the DSSC devices. Efficiencies on the order of 0.002% were calculated from these values. Overall, Dye 2 showed better performance with higher short circuit currents and open circuit voltages on average. This is the opposite trend observed in the data obtained from previous three-electrode photocurrent measurements, in which Dye 3 showed appreciably higher photocurrents compared to Dye 2. The current that goes into the oxidation of water by the catalyst in Dye 3 will not be shown in the DSSC measurements, therefore we expect lower currents when the catalyst is present. The lower photocurrent response of Dye 3 in these DSSCs was therefore promising in terms of the ability of Dye 3 to act as a catalyst for hydrogen evolution in DSPEC devices. All measurements were performed with no applied bias between the photoanode and the platinum cathode in these two electrode DSSC measurements, such that successful production of photocurrent at no applied bias has been proven possible.

Table 4. DSSC figures of merit for devices with Dye 2 and Dye 3					
Device	Dye	I_{sc} ($\mu A/cm^2$)	V_{OC} (mV)	Fill Factor (%)	Efficiency (%)
C	2	73	-134	23.8	0.00234
G	3	95	-49	24.2	0.00113

Conclusions

This study constructed core-shell nanoITO-STO substrates for use in DSSCs by a solution based method. An aqueous electrolyte was employed with a thiolate/disulfide redox couple in order to work towards integration in DSPEC water splitting devices. The core shell substrates showed photocurrent responses two to three orders of magnitude greater than corresponding flat STO previously reported. Constructed DSSCs showed low efficiencies overall, but proved that photocurrent response was possible with two-electrode measurements and no applied bias. Hydrogen production by the catalyst-dye molecule utilized needs to be further studied in order to incorporate this material into DSPEC devices.

Experimental

Film preparation

The nanoITO films were prepared through adaption of a method previously reported.[6] FTO glass (TEC-15, Hartford glass Co. Inc.) was cut to 2 cm x 4 cm and cleaned through sonication in ethanol two times for 20 minutes each. Kapton tape was used to cover a 2 cm x 2.5 cm area on one edge of the substrate. The nanoITO (Evonik) was then prepared by adding 1.5 g of nanoITO with 1.42 mL of acetic acid (Glacial, Fisher Scientific) to 5.0 mL ethanol (Decon, 200 Proof). The suspension was sonicated for 20 minutes. Ultrasonication was performed using a Branson ultrasonic horn flat microtip (30% power,

17% duty cycle; 5 minutes). Spin coating of the nanoITO suspension on the substrates was conducted at 600 rpm for 10 seconds. The films were then annealed in a Lindberg/Blue M Box Furnace under air at 500°C for 1 hour, with a one hour ramp to reach the annealing temperature, to produce light yellow oxidative nanoITO films.

Atomic layer deposition (ALD) was performed on the oxidative nanoITO films using a Cambridge NanoTech Savannah S200 instrument and trimethylaluminum precursor. Nitrogen gas was used in the chamber and an exposure mode treatment at 130°C was used to deposit 5 cycles of Al_2O_3 as follows: 0.02 s precursor pulse, 20 s hold, 60 s N_2 purge, 0.02 s H_2O pulse, 20 s hold, 60 s N_2 purge. An ALD film thickness of 0.8 nm was measured by ellipsometry (J. A. Woollam Variable Angle Spectroscopic Ellipsometer) on flat silicon wafer substrates co-deposited with the nanoITO films.

Synthesis of Dyes and Electrolyte

The thiolate/disulfide couple was synthesis according to literature procedure.[13] Dye 1 was synthesized according to a previously published procedure.[10] Dye 2 was synthesized by a previously published procedure.[12] Dye 3 was synthesized as a covalently linked assembly of the porphyrin and the catalyst based on a previously published procedure.[20]

STO and annealing

Strontium titanate (STO) films were created by drop casting a solution of strontium acetate, titanium (IV) isopropoxide (TTIP), ethyl alcohol (Sigma Aldrich) and acetic acid (Fisher). The ITO substrate was placed in a 100 mL jar and using a Fisherbrand Finnpipette, two runs of 75 μL of solution was slowly dropped onto the substrate for a total volume of 150 μL. Evaporation of the solution was regulated by capping the jar with a lid featuring an 11 mm aperture. The films were left to dry for approximately 18 hrs. Post deposition annealing was first done in air at 500°C for 60 min using a MTI Corporation box oven (model KSL-1200X) and then at 500°C in a 2% H_2 (Airgas) atmosphere for 120 min using a Lindberg/Blue tube furnace.

Device fabrication

DSSC construction was adapted from a literature method.[1] Films were prepared with the same method as indicated above for DSSCs. The area of the film was reduced to 0.5 cm^2 by scraping the surface with a razor blade in preparation for constructing sandwich type DSSCs with the other electrode being Pt coated FTO. The Pt was applied to clean pieces of 2 cm x 4 cm FTO, with a hole for injection of electrolyte, by applying a solution of Pt in ethanol to the FTO and sintering at 450°C, this process was repeated two times with cooling between. Surlyn film (Solaronix, 25 μm) was cut into a frame to act as a connector and spacer between electrodes and also used for sealing after electrolyte injection along with a cover glass. Connection of electrodes with Surlyn film was done through rapid heating to 150 °C in order to melt the polymer and ensure sealing. TDS electrolyte was used to fill these devices by vacuum backfilling, with the electrolyte being 0.1 M acetate buffer, pH 5, with additives to the electrolyte of 0.05 M thiolate/disulfide and 1% by volume Tritonx100.

The dyes were dissolved in dicholormethane/methanol (90:10 v:v) and films were loaded by dip coating for specific amounts of time.

Film characterization

SEM was conducted using a Hitachi S-4700 Cold Cathode Field Emission Scanning Electron Microscope with an accelerating voltage of 2.0 kV. Films were sputter coated (Cressington 108 Auto Sputter Coater) with 2.0 nm of Au/Pd before SEM. SEM EDS (Oxford instruments, INCA PentaFET -x3) was conducted with an accelerating voltage of 20.0 kV. TEM was conducted using a TEM JEOL 2010F-FasTEM with an accelerating voltage of 20.0 kV (EDS Oxford instruments, INCA Energy TEM 250). X-ray diffraction was conducted on the nanoITO films (Rigaku Multiflex, Source 1.5418 Å).

Electrochemistry:

Cyclic voltammetry (CV) and photocurrent measurements were made using a 601D CH Instruments potentiostat with a Pt wire reference and an aqueous Ag/AgCl (satd. NaCl, BASi) counter in aqueous 0.1 M acetate buffer, pH 5. Initial photocurrent measurements used Lumencor model Spectra light source (λmax = 445 nm, 20 nm FWHM, 75 mW/cm^2;

beam diameter = 0.8 cm) with RuP dye and in pH 1 (0.1 M $HClO_4$). TDS electrolyte was also used in these measurements. An AM1.5G (1 sun) solar simulator (Newport 1000W Xe lamp and an AM1.5G filter) illuminated the samples for CV and photocurrent measurements. Electrochemical impedance spectroscopy (EIS) curves were collected with a Gamry 500 potentiostat using Gamry Framework software. EIS was collected as two-electrode measurements with DSSCs. Incident photon-to-current conversion efficiencies (IPCE) were collected with a 75W Xe Oriel 6251/Photomax lamp housing/Oriel Cornerstone 260 monochromator, with light intensities tested with a calibrated Si-photodiode (UDT S370 optometer/260 detector) across all wavelengths. A Keithley 2400 sourcemeter collected photocurrent measurements and linear sweep voltammagrams (LSV). IPCE and LSV were conducted with a two-electrode measurement with DSSCs.

UV-Vis:

A Cary 50 UV-Vis spectrophotometer was used to record all absorbance spectra by placing the film or solution in the path of the beam with a fast scan rate, collecting data at every wavelength.

References

(1) Ito, S.; Murakami, T. N.; Comte, P.; Liska, P.; Grätzel, C.; Nazeeruddin, M. K.; Grätzel, M. *Thin Solid Films* **2008**, *516* (14), 4613–4619.

(2) Grätzel, M. *Nature* **2001**, *414* (6861), 338–344.

(3) Brennaman, M. K.; Dillon, R. J.; Alibabaei, L.; Gish, M. K.; Dares, C. J.; Ashford, D. L.; House, R. L.; Meyer, G. J.; Papanikolas, J. M.; Meyer, T. J. *J. Am. Chem. Soc.* **2016**, *138*, 13085–13102.

(4) Armaroli, N.; Balzani, V. *Chem. - A Eur. J.* **2016**, *22* (1), 32–57.

(5) Sherman, B. D.; Sheridan, M. V.; Wee, K.-R.; Marquard, S. L.; Wang, D.; Alibabaei, L.; Ashford, D. L.; Meyer, T. J. *J. Am. Chem. Soc.* **2016**, *138* (51), 16745–16753.

(6) Alibabaei, L.; Farnum, B. H.; Kalanyan, B.; Brennaman, M. K.; Losego, M. D.;

Parsons, G. N.; Meyer, T. J. *Nano Lett.* **2014**, *14* (6), 3255–3261.

(7) Wee, K.-R.; Sherman, B. D.; Brennaman, M. K.; Sheridan, M. V; Nayak, A.; Alibabaei, L.; Meyer, T. J. *J. Mater. Chem. A* **2016**, *4*, 2969–2975.

(8) Ganapathy, V.; Karunagaran, B.; Rhee, S.-W. *J. Power Sources* **2010**, *195*, 5138–5143.

(9) Wrighton, M. S.; Ellis, A. B.; Wolczanski, P. T.; Morse, D. L.; Abrahamson, H. B.; Ginley, D. S. *J. Am. Chem. Soc.* **1976**, *98* (10), 2774–2779.

(10) Call, R. W.; Alibabaei, L.; Dillon, R. J.; Knauf, R. R.; Nayak, A.; Dempsey, J. L.; Papanikolas, J. M.; Lopez, R. *ACS Appl. Mater. Interfaces* **2016**, *8* (19), 12282–12290.

(11) Knauf, R. R.; Kalanyan, B.; Parsons, G. N.; Dempsey, J. L. *J. Phys. Chem. C* **2015**, *119* (51), 28353–28360.

(12) Nayak, A.; Roy, S.; Sherman, B. D.; Alibabaei, L.; Lapides, A. M.; Brennaman, M. K.; Wee, K.-R.; Meyer, T. J. *ACS Appl. Mater. Interfaces* **2016**, *8*, 3853–3860.

(13) Fayad, R.; Shoker, T. A.; Ghaddar, T. H. *Dalt. Trans.* **2016**, *45*, 5622–5628.

(14) Boschloo, G.; Hagfeldt, A. *Acc. Chem. Res.* **2009**, *42* (11), 1819–1826.

(15) Varghese, J.; Ghoshal, T.; Deepak, N.; O'Regan, C.; Whatmore, R. W.; Morris, M. A.; Holmes, J. D. *Chem. Mater.* **2013**, *25* (8), 1458–1463.

(16) Reitz, C.; Leufke, P. M.; Hahn, H.; Brezesinski, T. *Chem. Mater.* **2014**, *26* (6), 2195–2202.

(17) Lee, S.-H. A.; Zhao, Y.; Hernandez-Pagan, E. A.; Blasdel, L.; Justin Youngblood, W.; Mallouk, T. E. *Faraday Discuss.* **2012**, *155*, 165–176.

(18) Sarker, S.; Ahammad, A. J. S.; Seo, H. W.; Kim, D. M. *Int. J. Photoenergy* **2014**, *2014*, 1–17.

(19) Bisquert, J.; Zaban, A.; Greenshtein, M.; Mora-Seró, I. *J. Am. Chem. Soc.* **2004**, *126*, 13550–13559.

(20) Nayak, A.; Hu, K.; Roy, S.; Gish, M.; Brennaman, M. K.; Meyer, G. J.; Meyer, T. J. *Manuscr. under Prep.*